


RESEARCH ARTICLE

Evaluation of [^{99m}Tc]Radiolabeled Macrophage Mannose Receptor-Specific Nanobodies for Targeting of Atherosclerotic Lesions in Mice

Gezim Bala ^{1,2} Henri Baudhuin,¹ Isabel Remory,^{1,3} Kris Gillis,^{1,2} Pieterjan Debie,¹ Ahmet Krasniqi,¹ Tony Lahoutte,^{1,4} Geert Raes,^{5,6} Nick Devoogdt,¹ Bernard Cosyns,^{1,2} Sophie Hernot¹

¹*In Vivo Cellular and Molecular Imaging (ICMI/BEFY), Vrije Universiteit Brussel, Brussels, Belgium*

²*Centrum voor Hart-en Vaatziekten (CHVZ), UZ Brussel, Brussels, Belgium*

³*Department of Anesthesiology, UZBrussel, Brussels, Belgium*

⁴*Nuclear Medicine Department, UZ Brussel, Brussels, Belgium*

⁵*Laboratory of Cellular and Molecular Immunology (CMIM), Vrije Universiteit Brussel, Brussels, Belgium*

⁶*Myeloid Cell Immunology Lab, VIB Inflammation Research Center, Ghent, Belgium*

Abstract

Purpose: Macrophage accumulation characterizes the development of atherosclerotic plaques, and the presence of certain macrophage subsets might be an indicator of plaque phenotype and (in)stability. The macrophage mannose receptor (MMR) is expressed on alternatively activated macrophages and found at sites of intraplaque hemorrhage and neovascularization. It has been proposed as target to identify vulnerable plaques. Therefore, we aimed to assess the feasibility of using anti-MMR nanobodies (Nbs) as molecular tracers for nuclear imaging in an animal model of atherosclerosis.

Procedure: Anti-MMR and control Nb, radiolabeled with Tc-99m, were injected in ApoE^{-/-} and/or C57Bl/6 mice ($n = 6$). *In vivo* competition studies involving pre-injection of excess of unlabeled anti-MMR Nb ($n = 3$) and injection of anti-MMR Nb in MMR^{-/-} mice ($n = 3$) were performed to demonstrate specificity. At 3 h p.i. radioactive uptake in organs, tissues and aorta segments were evaluated. Autoradiography and immunofluorescence were performed on aortic sections.

Results: Significantly higher uptake was observed in all aortic segments of ApoE^{-/-} mice injected with anti-MMR Nb compared to control Nb (1.36 ± 0.67 vs 0.38 ± 0.13 percent of injected dose per gram (%ID/g), $p \leq 0.001$). Surprisingly, high aortic uptake was also observed in C57Bl/6 mice ($1.50 \pm 0.43\%$ ID/g, $p \geq 0.05$ compared to ApoE^{-/-}), while aortic uptake was reduced to background levels in the case of competition and in MMR^{-/-} mice (0.46 ± 0.10 and $0.22 \pm 0.06\%$ ID/g, respectively; $p \leq 0.001$). Therefore, expression of MMR along healthy aortas was suggested. Autoradiography showed no specific radioactive signal within atherosclerotic plaques, but rather localization of the signal along the aorta, correlating with MMR expression in perivascular tissue as demonstrated by immunofluorescence.

Conclusions: No significant uptake of MMR-specific Nb could be observed in atherosclerotic lesions of ApoE^{-/-} mice in this study. A specific perivascular signal causing a non-negligible background level was demonstrated. This observation should be considered when using MMR

as a target in molecular imaging of atherosclerosis, as well as use of translational animal models with vulnerable plaques.

Key Words: Nanobody, Atherosclerosis, Macrophage mannose receptor, Molecular imaging

Introduction

Despite substantial advances in the field of cardiovascular medicine, it remains clinically challenging to prospectively identify individuals with a high likelihood of developing acute complications of atherosclerosis. A main focus has therefore been assigned to the development of non-invasive or minimally invasive imaging approaches to characterize atherosclerotic plaques. Molecular imaging has emerged as a promising tool to assess biological hallmarks involved in atherosclerotic plaque vulnerability. However, the selection of a specific biomarker implicated in culprit atherosclerotic lesions remains a major challenge of this approach [1].

Inflammation is generally recognized to play a prominent role in the development of atherosclerosis and its complications [2]. Indeed, macrophage accumulation and proliferation are involved in all stages of atherosclerosis, and macrophages are abundant, particularly in high-risk plaques [3]. As a result, many molecular imaging strategies attempt to image the presence of macrophages in atherosclerotic plaques [4]. Macrophages are heterogeneous populations of cells that can adapt their functional phenotype in response to specific signals from their direct environment (also known as macrophage polarization), and these different phenotypes can be distinguished based on the expression of surface markers and chemokine receptors [5]. Recent observations have demonstrated that the relative proportions of macrophage subsets within a plaque might be a better indicator of plaque phenotype and (in)stability than the total number of macrophages [6].

The macrophage mannose receptor (MMR) or CD206 is a C-type lectin-like receptor primarily present on the surface of a subset of macrophages [7]. Previous immunohistochemistry (IHC) studies in human coronary atherosclerosis have shown high MMR expression in thin-cap fibroatheroma (TCFA) [8], and this expression has been associated with neovascularization and intraplaque hemorrhage [9]. Although some controversies exist [10–12], MMR has been advocated as a potentially robust imaging target for high-risk atherosclerotic plaques [8]. Currently, several molecular imaging probes targeting MMR, such as 2-deoxy-2-[¹⁸F]fluoro-D-mannose (¹⁸F-FDM) and neomannosylated human serum albumin, are being evaluated in the context of atherosclerosis [8, 13, 14].

Nanobodies (Nbs) targeting MMR have previously been validated as potential tracers to target tumor-associated macrophages as an indicator of cancer progression and prognosis [15, 16], and to follow-up inflammatory responses in a mouse model of rheumatoid arthritis [17]. Indeed, Nbs,

which are small antigen-binding fragments derived from camelid heavy-chain-only antibodies and capable to recognize biomarkers involved in distinct diseases in a highly specific manner, enable the acquisition of high-contrast images in both animal models and patients, at early time points after injection [16–23]. We aimed to assess the feasibility of using the anti-MMR Nbs, labeled with Tc-99m, as molecular tracers for *in vivo* nuclear imaging in an animal model of atherosclerosis, using autoradiography and immunofluorescence staining as reference.

Methods

Animal Model

The animal study protocol was approved by the ethical committee for animal research of the Vrije Universiteit Brussel. Female (5-week-old) apolipoprotein E-deficient (ApoE^{-/-}) mice (Charles River, L'Arbresle, France) were fed a high-fat Western diet with 1.25 % cholesterol (D12108C, Research Diets, New Brunswick, NJ, USA) for 21–25 weeks to induce atherosclerotic lesions. Lesions develop all along the aorta, but are most prevalent in the region of the ascending aorta and aortic arch. Female healthy control C57Bl/6 (Charles River) and macrophage mannose receptor knockout (MMR^{-/-}) mice (kindly provided by Prof. E. Pays, ULB, Belgium) were used as control mice and remained on a standard chow diet.

Tc-99m Radiolabeling of Nanobodies

The Nb MMR3.49, recognizing both the mouse and human homolog of MMR, has previously been generated, validated, and selected as lead compound for further studies [16]. The non-targeting Nb cAbBCII10 was used as control compound [19]. The Nbs were labeled with Tc-99m *via* their hexahistidine tail using Tc-99m tricarbonyl chemistry as described elsewhere [24]. Final radiochemical purity was > 98 %.

SPECT/CT Imaging and Ex Vivo Biodistribution Analysis

Of [^{99m}Tc]anti-MMR3.49 Nb (~5 µg), 30–70 MBq was injected intravenously *via* the tail vein in ApoE^{-/-} (*n* = 6), C57Bl/6 (*n* = 3), and MMR^{-/-} mice (*n* = 3). In addition, ApoE^{-/-} mice (*n* = 6) injected with [^{99m}Tc]cAbBCII10, and C57Bl/6 mice (*n* = 3) pre-injected 15 min before with 100-

fold molar excess of unlabeled MMR3.49 Nb, were used to demonstrate specific uptake.

At 180 min post-injection, mice were anesthetized using ketamine hydrochloride (CEVA, 75 mg/kg) and medetomidine hydrochloride (Domitor, Pfizer, 0.5 mg/kg) and subjected to a micro-SPECT (e.cam¹⁸⁰, Siemens, USA) equipped with a triple 1-mm pinhole collimator (30 s per projection, 64 projections, total scan time 40 min) and micro-CT (Skyscan 1178, Bruker) scan according to standard protocols [21]. Image analysis was performed using AMIDE medical imaging software.

After SPECT/CT imaging, the mice were euthanized with a lethal dose of pentobarbital (Ceva). Organs and tissues of interest were collected, including the aorta that was dissected from aortic root to iliac bifurcation and cut into 8–10 segments. The aorta segments were analyzed on a stereomicroscope, and a lesion extension score was given according to plaque burden: score 0—no lesion, score 1—lesion covering up to 30 % of the segment, score 2—lesions covering 30–75 % of the segment, and score 3—lesions extending over the whole segment. All organs, tissues, and aorta segments were then weighed and counted for radioactivity against a standard of known activity. Uptake was expressed as percentage of injected dose per gram (%ID/g), corrected for decay [20].

Autoradiography

Segments of the aortic arch and thoracic aorta of ApoE^{-/-}, C57Bl/6, and MMR^{-/-} mice ($n = 3$ per group) injected with [^{99m}Tc]anti-MMR3.49 were flash frozen in Tissue-Tek OCT compound (Sakura, USA). Five-micrometer-thick transversal sections were prepared using a cryotome (FSE Cryotome, Life Technologies, Grand Island, NY, USA) and placed on a microscope slide (Superfrost Plus, Thermofischer Scientific, Germany). The slides were exposed overnight to a radio-sensitive screen (BAS-IP SR) and analyzed using the Typhoon FLA 7000 system (GE Healthcare, Freiburg, Germany).

Immunofluorescence Staining of MMR and CD68

Five-micrometer-thick transversal cryosections of the aortic arch and thoracic aorta of ApoE^{-/-} ($n = 26$ segments), C57Bl/6 ($n = 3$ segments), and MMR^{-/-} ($n = 3$ segments) mice were prepared as described above. The sections were first fixated in ice-cold acetone (Sigma-Aldrich), and non-specific binding sites were blocked with 4 % donkey serum (D-9663; Sigma-Aldrich) for 30 min. The sections were then incubated overnight at 4 °C with either rabbit anti-mouse CD206 polyclonal antibody (5 µg/mL, ab64693, Abcam) or rat monoclonal antibody to CD68 (20 µg/mL; MCA1957; Bio-Rad). After washing three times with PBS for 5 min, the slides were incubated with a secondary fluorescently labeled antibody for 1 h in the dark at room temperature: donkey

anti-rabbit IgG AF488 (10 µg/mL; A21206, Invitrogen) and goat anti-rat IgG FITC (2 µg/mL; SC-2011, Santa Cruz) for CD206 and CD68 staining, respectively. Afterwards, slides were washed twice with PBS, rinsed with dH₂O, mounted, and counterstained with Vectashield supplemented with 4',6-diamidino-2-phenylindole (DAPI) (H-1200; Vector Laboratories). Images were acquired with a fluorescence microscope (EVOS Fl, Thermofisher Scientific) using the GFP and DAPI light cubes, and a 10× objective (Plan Fluor AMEP-4623).

Statistical Analysis

Data are expressed as mean ± standard deviation. Variables were tested for homogeneity of variance by the Levene's test. Comparisons between groups were performed using one-way ANOVA tests, corrected for multiple comparisons using contrast coefficients. A p - value ≤ 0.05 was considered significant. Statistical analysis was done using SPSS Statistics software (version 24.0.0, IBM Company, Chicago, IL, USA).

Results

In Vivo and Ex Vivo Organ and Tissue Biodistribution

The biodistribution of [^{99m}Tc]Nb MMR3.49 in ApoE^{-/-}, C57Bl/6, and MMR^{-/-} mice and [^{99m}Tc]cAbBCII10 in ApoE^{-/-} is represented in Fig. 1a, b. Tc-99m-labeled Nbs are rapidly cleared from the circulation *via* renal excretion as demonstrated by low blood values (< 0.5%ID/g) and high kidney values for all experimental groups at 3 h p.i. Additionally, significantly higher uptake of [^{99m}Tc]Nb MMR3.49 was observed in several organs and tissues (liver, spleen, heart, thymus, bone, and lymph nodes) compared to the uptake of [^{99m}Tc]cAbBCII10. These uptakes were demonstrated to be the result of specific targeting as signals were significantly reduced by pre-injecting excess of unlabeled Nb MMR3.49, and as MMR^{-/-} mice showed only background uptake in these organs and tissues. No hotspots could be distinguished at the level of the aortic arch (region where most of the segments are scored as 3) in ApoE^{-/-} mice injected with [^{99m}Tc]Nb MMR3.49.

Uptake in Aortic Segments

Based on *ex vivo* analysis, uptake of [^{99m}Tc]Nb MMR3.49 in all aortic segments of ApoE^{-/-} mice was significantly higher compared to ApoE^{-/-} mice injected with a control Nb ([^{99m}Tc]cAbBCII10), regardless of the extent of atherosclerosis (Fig. 2a) (1.36 ± 0.67 vs $0.38 \pm 0.13\%$ ID/g, $p < 0.001$). Surprisingly, [^{99m}Tc]Nb MMR3.49 also showed a high uptake in aorta segments of healthy C57Bl/6 mice ($1.50 \pm 0.43\%$ ID/g), which was comparable with uptake in

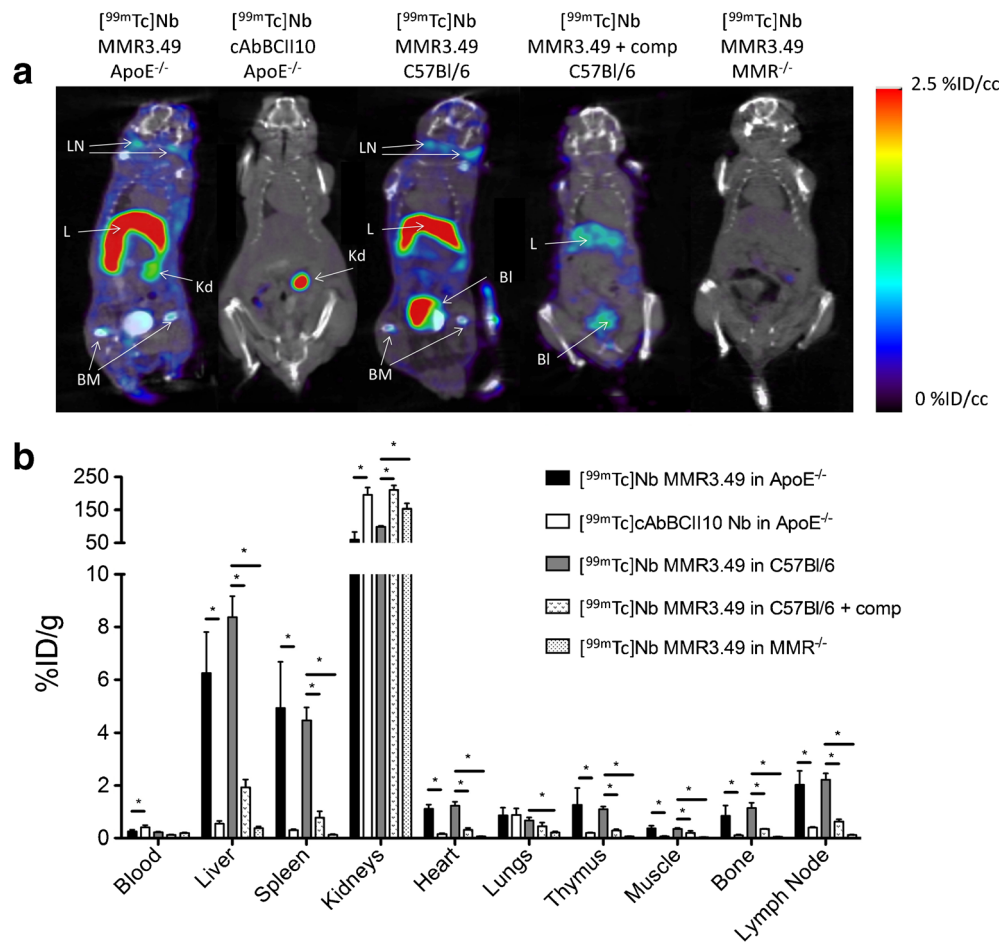


Fig. 1. **a** SPECT/CT images and **b** *ex vivo* biodistribution data of [^{99m}Tc]Nb MMR3.49 in ApoE^{-/-} ($n = 6$), in C57Bl/6 ($n = 6$), in C57Bl/6 mice pre-injected with an excess of unlabeled Nb MMR3.49 ($n = 3$), and in MMR^{-/-} mice ($n = 3$), as well as [^{99m}Tc]cAbBCII10 in C57Bl/6 ($n = 6$). Coronal views are shown at the level of the aortic arch. All images are scaled to the same level. LN lymph node, L liver, Kd kidney, BM bone marrow, Bl bladder. * $p \leq 0.05$. (Color figure online).

aorta segments of ApoE^{-/-} mice without visible atherosclerotic lesions (score $0.201 \pm 0.85\%ID/g$; $p > 0.05$) (Fig. 2a).

To further investigate whether the uptake of [^{99m}Tc]Nb MMR3.49 at the level of normal vessels was due to specific targeting, additional experiments were performed including competition studies and MMR^{-/-} mice. In both of these groups, binding of [^{99m}Tc]Nb MMR3.49 in normal aortic segments was significantly reduced (0.46 ± 0.10 and $0.22 \pm 0.06\%ID/g$, respectively) compared to C57Bl/6 mice ($1.50 \pm 0.43\%ID/g$, $p \leq 0.001$), demonstrating specific uptake of [^{99m}Tc]-Nb MMR3.49 along the aorta of C57Bl/6 mice (Fig. 2b).

Autoradiography

Autoradiography of cryosections of the aortic root (coronal sections including some myocardial tissue) as well as thoracic aorta segments (transversal sections) revealed high radioactive signals in the perivascular region of the aorta as well as in myocardial tissue of ApoE^{-/-} and C57Bl/6 mice. In contrast, only low signal was detected for MMR^{-/-} mice.

Importantly, no increased signal was visible at the level of atherosclerotic plaque lesions (Fig. 3).

Immunofluorescence

Immunofluorescence staining showed the presence of perivascular expression of MMR along the aorta of ApoE^{-/-} and C57Bl/6 mice, in particular at the origin of the branches of the aortic arch (Fig. 4). No MMR expression was found in MMR^{-/-} mice.

Despite the presence of CD68-positive cells, no MMR expression could be demonstrated within atherosclerotic lesions. However, focal expression of MMR, differing in degree, in the adventitial layer was found adjacent to intimal lesions (Fig. 5).

Discussion

Motivated by recent findings showing predominant expression of MMR in thin-capped fibroatheroma with neovascularization and intraplaque hemorrhages [8, 9],

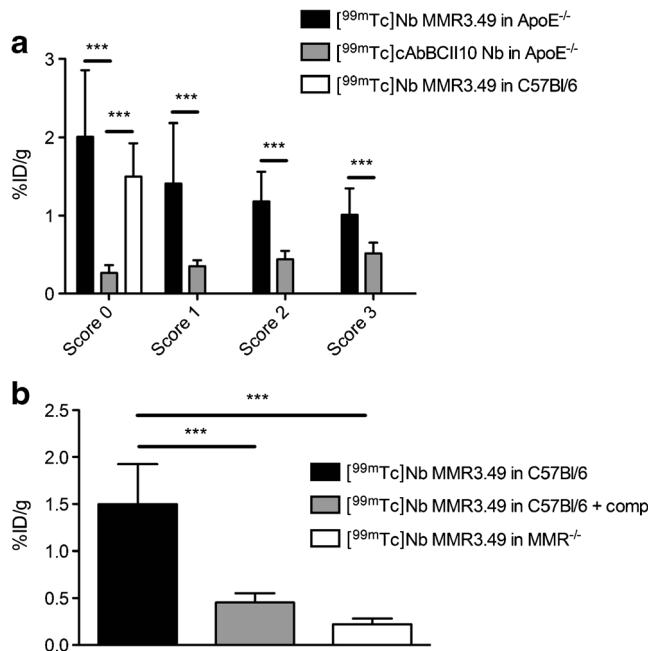


Fig. 2. a Uptake, according to extent of plaque burden, in aortic segments of ApoE^{-/-} ($n = 6$) and C57Bl/6 ($n = 6$) mice injected with [^{99m}Tc]Nb MMR3.49 and of ApoE^{-/-} mice ($n = 6$) injected with [^{99m}Tc]cAbBCII10. *** $p \leq 0.001$. **b** Uptake of [^{99m}Tc]Nb MMR3.49 in aortic segments of C57Bl/6 ($n = 6$), MMR^{-/-}, or C57Bl/6 mice pre-injected with 100-fold excess of unlabeled Nb MMR3.49 ($n = 3$). *** $p \leq 0.001$.

MMR has been proposed as potential marker to specifically identify high-risk atherosclerotic lesions. Therefore, in the current study, we aimed to investigate the feasibility of imaging MMR expression in a murine model of atherosclerosis using radiolabeled Nbs.

In the utilized model of atherosclerosis, namely ApoE^{-/-} mice on a Western diet, no positive correlation was found between plaque burden and tracer uptake.

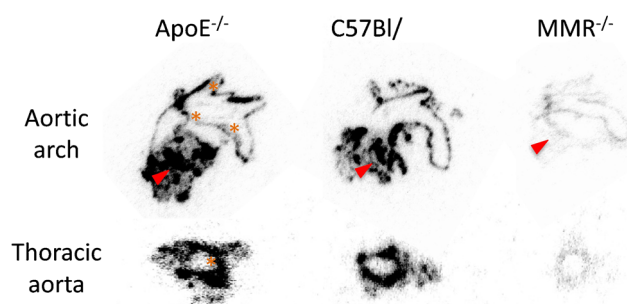


Fig. 3. Autoradiography of aortic arch with myocardium (coronal sections) and thoracic aorta (transversal sections) of ApoE^{-/-}, C57Bl/6, and MMR^{-/-} mice injected with [^{99m}Tc]Nb MMR3.49. A high radioactive signal was observed in aortic regions of ApoE^{-/-} and C57Bl/6 mice, while minimal signal was observed in aortic sections of MMR^{-/-} mice. There was no increased signal in areas with plaque (orange asterisk indicates area with plaque; red arrow indicates myocardium). (Color figure online).

Although the extent of atherosclerosis does not necessarily reflect the inflammatory status of plaques, the absence of specific uptake of anti-MMR Nb in atherosclerotic lesions corroborated with the absence of MMR expression as shown by immunofluorescence staining (despite the presence of CD68-positive inflammatory cells). Remarkably, specific targeting of MMR was demonstrated in peri-aortic tissues of both ApoE^{-/-} and C57Bl/6 mice, resulting in non-negligible background signal in close proximity of the plaques. The presence of MMR-positive macrophages lining the vascular adventitia has previously been reported by Stöger et al. [25], although their exact role in homeostasis still remains unclear. Additionally, at sites of plaque formation, we also observed perivascular regions containing an increased number of cells that stained positive for MMR. This is in accordance with the described presence of adventitial cellular infiltration related to atheroma [26] or could be attributed to the presence of perivascular lymph nodes.

Biodistribution analysis confirmed relatively high specific uptake of Tc-99m-labeled anti-MMR Nbs in several organs, among which are the liver, spleen, heart, thymus, bone marrow, and lymph nodes [15]. The presence of tissue-resident MMR-positive macrophages, as well as other cells such as hepatic and lymphatic endothelial cells that express MMR on their cell surface, is well described for these tissue and organs [27]. These observations indicate that the diffuse distribution of MMR-expressing cells, and in particular along normal vessels and in myocardial tissue, might be a limitation for molecular imaging of this biomarker in the context of atherosclerosis, especially for coronary heart disease. Nevertheless, we have previously shown that targeting of constitutively expressing organs was significantly lower when an excess of bivalent anti-MMR nanobody was co-injected [15] or when fluorinated analogs of the Nbs were used instead of the Tc-99m-labeled ones, while targeting of the disease of interest was preserved [16, 20]. It is thus possible that this limitation might be overcome using a different tracer formulation or radiochemistry, although possible explanations so far remain speculative.

Other groups have previously described molecular imaging strategies targeting mannose receptor in both rabbit and mice models of atherosclerosis, using either [¹⁸F]FDM, Ga-68-labeled NOTA-neomannosylated human serum albumin, or Cy5.5/7-labeled MMR targeting nanoparticles as molecular tracers [8, 13, 14]. They all reported specific uptake of their molecular tracer in atherosclerotic lesions based on both *in vivo* and *ex vivo* data with low background signals in healthy animals. It should be mentioned that MMR expression in atherosclerotic lesions and perivascular tissues of their respective animal models was not investigated. Provided that the signals observed in the abovementioned models are

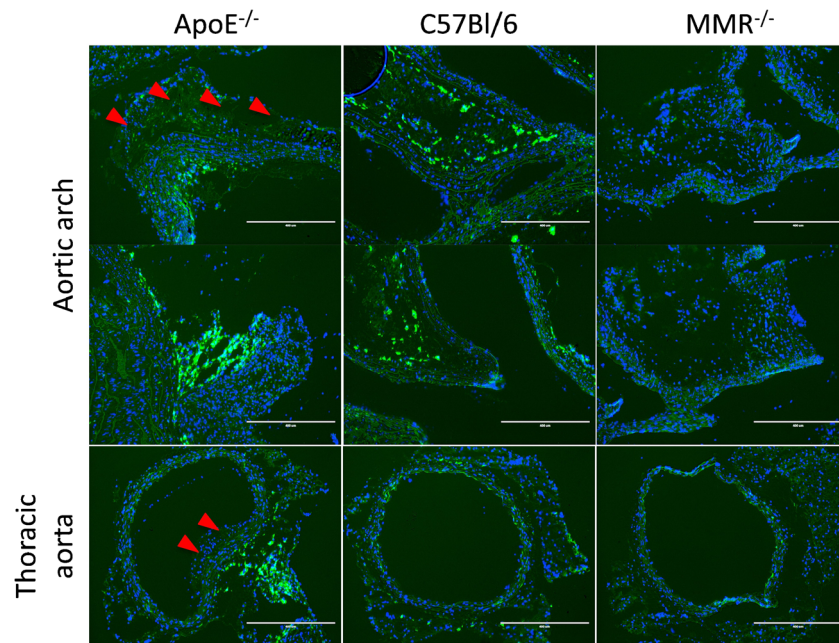


Fig. 4. Photomicrographs of MMR staining in aortic tissue sections (aortic arch and thoracic aorta) of ApoE^{-/-}, C57Bl/6, and MMR^{-/-} mice showing MMR expression in peri-aortic regions of both ApoE^{-/-} and C57Bl/6 mice, while no MMR expression is observed in plaque area or in MMR^{-/-} mice. *Red arrows* indicate plaque areas. (Color figure online).

indeed due to binding to MMR, this indicates that in case the atherosclerotic lesions do exhibit a strong MMR-positive phenotype, the background signals can be surmounted. Discrepancy in MMR expression in plaques between our results and other preclinical data could be caused by differences in duration or aggressiveness of the diet used, as well as the age of the animals, though MMR expression in murine models of atherosclerosis is not well described in literature. The use of models with a more inflamed and vulnerable plaque phenotype (e.g., plaque rupture, intraplaque neovascularization

and bleeding...), such as surgically cuffed arteries [28] or HypoE/SRBI^{-/-} [29] and ApoE^{-/-}Fbn1^{C1039G+/-} transgenic mice [30], could offer a better alternative to investigate the potential of MMR-targeted tracers for the purpose.

The dissimilarities between experimental and clinical conditions, particularly regarding plaque characteristics and evolution, composition, and evolution, emphasize again the importance of more translational animal models for vulnerable plaques. Yet, the contribution of MMR-positive macrophages in the evolution and vulnerability of atherosclerotic plaques, even in humans, still remains a matter of

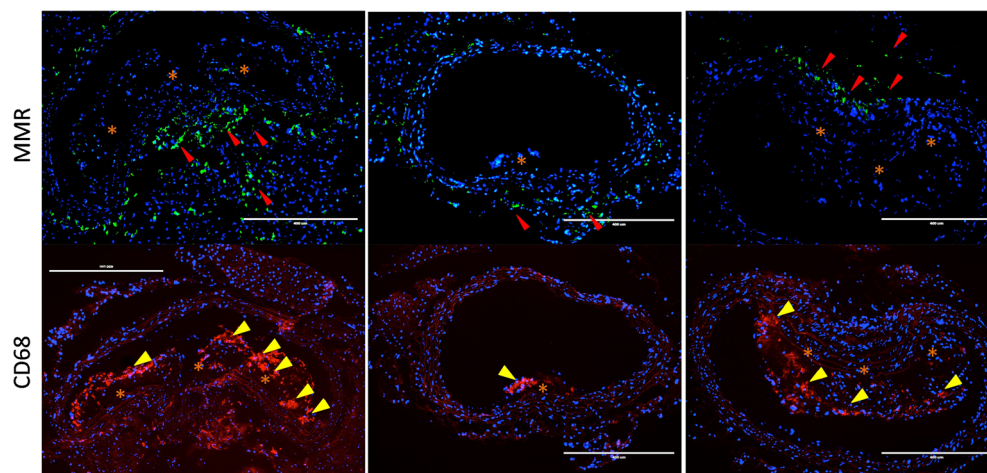


Fig. 5. Photomicrographs of MMR (*green signal*) and CD68 (*red signal*) staining on adjacent aortic sections of ApoE^{-/-} mice. DAPI-stained nuclei are shown in *blue*. *Red arrows* indicate MMR expression. *Yellow arrows* denote the presence of CD68-expressing macrophages. *Orange asterisk* indicates plaque area showing no intraplaque MMR expression, while these plaques exhibit infiltration of CD68-expressing macrophages. (Color figure online).

debate [11, 12]. On one hand, MMR expression has been described on macrophages referred to as M(Hb), involved in the clearance of hemoglobin-haptoglobin complexes after plaque hemorrhage [9]. On the other hand, alternatively activated, M2 macrophages with an anti-inflammatory phenotype, found in areas distant from both the lipid core and hemorrhagic zones, also express MMR [10].

The exact role of the distinct macrophage subpopulations, and in particular their relative predominance in relation to plaque vulnerability/stability, thus needs to be further elucidated. Nevertheless, as inflammation is a major criterion for vulnerability, imaging of macrophage content, and in particular their phenotypic characteristics remains an attractive road in the context of plaque imaging and therapy.

Conclusion

Although we were not able to evaluate the relevance of MMR targeting with radiolabeled Nbs in this mouse model of atherosclerosis, we demonstrated specific perivascular signal causing a non-negligible background level. This limitation, in addition to the diffuse presence of MMR-expressing cells in several organs and tissues, and the distinct roles MMR-positive macrophages play in the pathogenicity of atherosclerosis, should be taken into account when using MMR as target in molecular imaging of atherosclerosis. Furthermore, importance should also be given to animal models reflecting the clinical situation, in order to assess the true value of the tracer for patients.

Acknowledgements. We thank Cindy Peleman for her technical assistance.

Funding This research has been supported by a grant of Research Foundation—Flanders (FWO), Scientific Fund Willy Gepts—UZ Brussel, Strategic Basic Research (Strategisch Basis Onderzoek—Inflammatrack (SBO)), and Industrial Research Fund (Industrieel OnderzoeksFonds (IOF)).

Compliance with Ethical Standards

Conflict of Interest

Drs. Henri Baudhuin, Isabel Remory, Kris Gillis, Pieterjan Debie, Ahmet Krasniqi, and Bernard Cosyns declare that they have no conflict of interest. Vrije Universiteit Brussel (including Drs. Gezim Bala, Tony Lahoutte, Geert Raes, Nick Devoogdt, and Sophie Hernot) has a patent issued (US20160024213A1) regarding anti-macrophage mannose receptor single variable domains for use in cardiovascular diseases.

References

- Quillard T, Libby P (2012) Molecular imaging of atherosclerosis for improving diagnostic and therapeutic development. *Circ Res* 111:231–244
- Libby P, Ridker PM, Maseri A (2002) Inflammation and atherosclerosis. *Circulation* 105:1135–1143
- Libby P (2012) Inflammation in atherosclerosis. *Arterioscler Thromb Vasc Biol* 32:2045–2051
- Tarkin JM, Joshi FR, Rudd JHF (2014) PET imaging of inflammation in atherosclerosis. *Nat Rev Cardiol* 11:443–457
- Colin S, Chinetti-Gbaguidi G, Staels B (2014) Macrophage phenotypes in atherosclerosis. *Immunol Rev* 262:153–166
- Chinetti-Gbaguidi G, Colin S, Staels B (2015) Macrophage subsets in atherosclerosis. *Nat Rev Cardiol* 12:10–17
- Gordon S (2003) Alternative activation of macrophages. *Nat Rev Immunol* 3:23–35
- Tahara N, Mukherjee J, de Haas HJ et al (2014) 2-Deoxy-2-[¹⁸F]fluoro-D-mannose positron emission tomography imaging in atherosclerosis. *Nat Med* 20:215–219
- Finn AV, Nakano M, Polavarapu R et al (2012) Hemoglobin directs macrophage differentiation and prevents foam cell formation in human atherosclerotic plaques. *J Am Coll Cardiol* 59:166–177
- Chinetti-Gbaguidi G, Baron M, Bouhlef MA et al (2011) Human atherosclerotic plaque alternative macrophages display low cholesterol handling but high phagocytosis because of distinct activities of the PPAR γ and LXR α pathways. *Circ Res* 108:985–995
- Finn AV, Saeed O, Virmani R (2012) Macrophage subsets in human atherosclerosis. *Circ Res* 110:1–8
- Chinetti-Gbaguidi G, Staels B (2012) Response to the letter by Finn et al. *Circ Res* 110:e65–e66
- Kim EJ, Kim S, Seo HS et al (2016) Novel PET imaging of atherosclerosis with ⁶⁸Ga-labeled NOTA-neomannosylated human serum albumin. *J Nucl Med* 57:1792–1797
- Kim JB, Park K, Ryu J et al (2016) Intravascular optical imaging of high-risk plaques in vivo by targeting macrophage mannose receptors. *Sci Rep* 6:22608
- Movahedi K, Schoonooghe S, Laoui D et al (2012) Nanobody-based targeting of the macrophage mannose receptor for effective in vivo imaging of tumor-associated macrophages. *Cancer Res* 72:4165–4177
- Blykers A, Schoonooghe S, Xavier C et al (2015) PET imaging of macrophage mannose receptor-expressing macrophages in tumor stroma using ¹⁸F-radiolabeled camelid single-domain antibody fragments. *J Nucl Med* 56:1265–1271
- Put S, Schoonooghe S, Devoogdt N et al (2013) SPECT imaging of joint inflammation with nanobodies targeting the macrophage mannose receptor in a mouse model for rheumatoid arthritis. *J Nucl Med* 54:807–814
- Broisat A, Hernot S, Toczek J et al (2012) Nanobodies targeting mouse/human VCAM1 for the nuclear imaging of atherosclerotic lesions. *Circ Res* 110:927–937
- Vaneycken I, Devoogdt N, Van Gassen N et al (2011) Preclinical screening of anti-HER2 nanobodies for molecular imaging of breast cancer. *FASEB J* 25:2433–2446
- Bala G, Blykers A, Xavier C et al (2016) Targeting of vascular cell adhesion molecule-1 by ¹⁸F-labelled nanobodies for PET/CT imaging of inflamed atherosclerotic plaques. *Eur Hear J - Cardiovasc Imaging* 17:1001–1008
- De Vos J, Mathijs I, Xavier C et al (2014) Specific targeting of atherosclerotic plaques in ApoE^{-/-} mice using a new camelid sdAb binding the vulnerable plaque marker LOX-1. *Mol Imaging Biol* 16:690–698
- Zheng F, Devoogdt N, Sparkes A et al (2015) Monitoring liver macrophages using nanobodies targeting Vsig4: concanavalin A induced acute hepatitis as paradigm. *Immunobiology* 220:200–209
- Keyaerts M, Xavier C, Heemskerk J et al (2016) Phase I study of ⁶⁸Ga-HER2-nanobody for PET/CT assessment of HER2 expression in breast carcinoma. *J Nucl Med* 57:27–33
- Xavier C, Devoogdt N, Hernot S et al (2012) Site-specific labeling of his-tagged Nanobodies with ^{99m}Tc: a practical guide. *Methods Mol Biol* 911:485–490
- Stöger JL, Gijbels MJJ, van der Velden S et al (2012) Distribution of macrophage polarization markers in human atherosclerosis. *Atherosclerosis* 225:461–468
- Schwartz CJ, Mitchell JR (1962) Cellular infiltration of the human arterial adventitia associated with atheromatous plaques. *Circulation* 26:73–78
- Linehan SA, Martínez-Pomares L, Stahl PD, Gordon S (1999) Mannose receptor and its putative ligands in normal murine lymphoid and nonlymphoid organs: in situ expression of mannose receptor by selected macrophages, endothelial cells, perivascular microglia, and mesangial cells, but not dendritic cells. *J Exp Med* 189:1961–1972

28. Lardenoye JH, Delsing DJ, de Vries MR et al (2000) Accelerated atherosclerosis by placement of a perivascular cuff and a cholesterol-rich diet in ApoE*3Leiden transgenic mice. *Circ Res* 87:248–253
29. Zhang S, Picard MH, Vasile E et al (2005) Diet-induced occlusive coronary atherosclerosis, myocardial infarction, cardiac dysfunction, and premature death in scavenger receptor class B type I-deficient, hypomorphic apolipoprotein ER61 mice. *Circulation* 111:3457–3464
30. Van der Donckt C, Van Herck JL, Schrijvers DM et al (2015) Elastin fragmentation in atherosclerotic mice leads to intraplaque neovascularization, plaque rupture, myocardial infarction, stroke, and sudden death. *Eur Heart J* 36:1049–1058